Transferability of the SRP32-vdW specific reaction parameter functional to CHD_3 dissociation on Pt(110)-(2x1)

Helen Chadwick[1*†], Ana Gutiérrez-González[2], Rainer D. Beck[2] and Geert-Jan Kroes[1]

1. Leiden Institute of Chemistry, Gorlaeus Laboratories, Leiden University, P.O. Box 9502, 2300 RA Leiden, The Netherlands.

2. Laboratoire de Chimie Physique Moléculaire, Ecole Polytechnique Fédérale de Lausanne, CH-1015 Lausanne, Switzerland.

†. Current address. Department of Chemistry, Swansea University, Singleton Park, Swansea, SA2 8PP, United Kingdom.

Stepped transition metal surfaces, including the reconstructed Pt(110)-(2x1) surface, can be used to model the effect of line defects on catalysts. We present a combined experimental and theoretical study of CHD_3 dissociation on this surface. Theoretical predictions for the initial sticking coefficients, S_0, are obtained from *ab-initio* molecular dynamics calculations using the specific reaction parameter (SRP) approach to density functional theory, while the measured sticking coefficients were obtained using the King and Wells method. The SRP density functional (DF) used here had been previously derived for methane dissociation on Pt(111), so that the experiments test the transferability of this SRP DF to methane + Pt(110)-(2x1). The agreement between the experimental and calculated S_0 is poor, with the average energy shift between the theoretical and measured reactivities being 20 kJ/mol. There are two factors which may contribute to this difference, the first of which is that there is a large uncertainty in the calculated sticking coefficients due to a large number of molecules being trapped on the surface at the end of the 1 ps propagation time. The second is that the SRP32-vdW functional may not accurately describe the Pt(110)-(2x1) surface. At the lowest incident energies considered here, Pt(110)-(2x1) is more reactive than the flat Pt(111) surface, but the situation is reversed at incident energies above 100 kJ/mol.

***** Email address: h.j.chadwick@swansea.ac.uk

I. Introduction

The dissociation of gas phase molecules on transition metal surfaces often represents the rate controlling step in heterogeneously catalyzed processes[1]. To be able to describe these reactions theoretically, an accurate method of calculating the activation barrier for the dissociation is required. For gas-surface reactions, generalized gradient approximation (GGA) functionals are usually used within density functional theory[2–10] (DFT), although the mean unsigned error of the activation barrier obtained using these functionals is almost 16 kJ/mol even for simpler, gas phase reactions[11]. Whilst this value has not been determined for gas-surface reactions, the activation barriers for dissociation found using typical GGA functionals are not chemically accurate (correct to within 4.2 kJ/mol)[12]. As a result of the limited accuracy of GGA-DFT, dynamics calculations[2,4,5,13–16] based on models of the molecule-surface interaction employing standard GGA functionals such as the PBE functional[17,18] tend to reproduce sticking probabilities of molecules on metals only semi-quantitatively.

One semi-empirical method for obtaining a chemically accurate value of the activation barrier is to use a weighted average of two GGA functionals, one which underestimates the activation barrier (e.g., PBE[17,18] or PW91[19]) and one which overestimates the activation barrier (e.g., RPBE[20]). The weighting of the two functionals in the average is adjusted so that calculations using this so called specific reaction parameter (SRP) functional reproduce reactivities determined from a set of molecular beam experiments[15,21]. It is then tested against the results of other experiments on the same system but run under different conditions which were not originally used to determine the weighting, for example experiments involving a specific initial molecular vibrational state. If the calculated sticking coefficients also reproduce these additional experiments within chemical accuracy, this validates the functional as an SRP functional.

Whilst it has been shown that such an SRP approach can provide chemically accurate activation barriers for a number of gas-surface reactions[15,21–25], how transferable these SRP functionals are to different (related) systems remains an open question. The first demonstration of the transferability of an SRP functional between different planes of a transition metal surface was that the SRP functional for H_2 dissociation on Cu(111)[15] also reproduced the experimental dissociation probabilities for H_2 on Cu(100)[22]. However it was found that a slightly modified version of this functional which still correctly modelled H_2 dissociation on Cu(111)[25] does not give a chemically accurate description for D_2 dissociation on Ag(111)[26]. It was suggested that this was due to the functional not including van der Waals correlation, which has been shown to be necessary previously for giving accurate descriptions of dissociation dynamics[14,27].

The transferability of an SRP functional amongst different metals of the same group (group 10) of the periodic table has been demonstrated for methane dissociation, where the same SRP functional gives a chemically accurate description for the reaction of methane on Ni(111)[21,23,28], Pt(111)[23] and Pt(211)[23,29,30]. This same SRP functional has recently been used to predict the reactivity of CHD_3 on Cu(111) and Cu(211)[31], and when experimental data becomes available this will confirm whether the SRP functional is also transferable to methane dissociation on transition metals in other specific groups of the periodic table. The transferability of an SRP functional for a specific molecule reacting on a flat surface of a specific metal to that molecule interacting with a stepped surface of that metal is important for the accurate simulation of heterogeneously catalyzed reactions, and can help with bridging the so-called structure gap in heterogeneous catalysis[23].

In the present work, we study the dissociative chemisorption of trideuterated methane on Pt(110)-(2x1), comparing results from *ab-initio* molecular dynamics (AIMD) calculations with those from King and Wells beam reflectivity measurements. At a surface temperature of

650 K, as used in the present study, Pt(110) undergoes a missing row reconstruction[32] and is therefore a stepped surface[33]. The structure of the missing row reconstructed Pt(110)-(2x1) is shown schematically in Fig. 1. We refer to the three inequivalent rows of atoms in the surface as ridge, facet and valley, as shown in Fig. 1A, to be consistent with the notation used in previous work[34], and note that the ridge atoms have the same co-ordination number as the step atoms in the Pt(211) surface. Unlike ordinary stepped surfaces, it is not possible to distinguish between steps and terraces on Pt(110)-(2x1), but the rows of under co-ordinated ridge atoms may be viewed as step edges protruding from the surface. The x-axis is defined as being perpendicular to the three rows of atoms in the surface, the y-axis runs parallel to these atomic rows and the z-axis corresponds to the surface normal.

The dissociative chemisorption of methane on Pt(110)-(2x1) has been studied theoretically by Jackson and co-workers[35], who obtained reaction barriers in the range 65-70 kJ/mol with DFT using the PBE functional[17,18], which were lower than PBE barriers for methane dissociation on Pt(111). Reaction paths relevant to methane dissociation on Pt(110)-(2x1) were studied with DFT by King and co-workers[36–38].

McMaster and Madix studied dissociation of CH_4 on Pt(110)-(2x1) experimentally, using supersonic molecular beam experiments[39]. For normal incidence and kinetic energies in the range 75-110 kJ/mol, sticking probabilities in the range 0.04-0.12 were obtained. For energies exceeding 75 kJ/mol, they found Pt(111) to be far more reactive towards CH_4 dissociation than Pt(110)-(2x1). Also using supersonic molecular beams, Walker and King[40,41] found the dissociation probability to increase with decreasing incident energy for kinetic energies less than about 10 kJ/mol. This finding was reproduced in molecular beam experiments by Bisson et al.[42], who attributed this to a trapping mediated mechanism, where the trapping was called diffraction mediated, i.e., attributed to energy transfer from motion normal to the surface to motion parallel to the surface. In contrast to McMaster and Madix,

they found the Pt(111) surface to be less reactive towards CH_4 dissociation than the Pt(110)-(2x1) surface, albeit they addressed a different range of normal incident energies (up to 65 kJ/mol). Their work suggested the barrier to methane dissociation to be about 14 kJ/mol lower on Pt(110)-(2x1) than on Pt(111). The study of the dependence of the sticking probability on incidence angle and incidence plane suggested that methane dissociation on Pt(110)-(2x1) occurs predominantly on the ridge sites[42]. Finally, Bisson et al. also studied the initial vibrational state dependence of sticking of CH_4 to Pt(110)-(2x1), finding that combining stretch excitation with bend excitation is most conducive to increasing the reactivity[43].

Dynamics calculations addressed the initial vibrational state dependence of methane dissociation on Pt(110)-(2x1) by studying the reverse reaction (associative desorption) and invoking detailed balance[44,45]. Using a quantum dynamical method (the reaction path Hamiltonian method) and a PBE-DFT[17,18] model for the CH_4 + Pt(110)-(2x1) interaction, Jackson and co-workers were able to obtain a correct description of the dependence of sticking on surface temperature, but their results only semi-quantitatively reproduced the dependence of the sticking probability on incident energy[33].

In the present work, we continue to test the transferability of the SRP functional originally developed to describe dissociative chemisorption of CHD_3 on Ni(111)[21] and Pt(111)[23], to CHD_3 dissociation on the stepped Pt(110)-(2x1) surface. We selected CHD_3 rather than CH_4 as our intention was originally to also look at initial-state selective reaction, which AIMD is capable of describing for CHD_3 (with the C-H stretch pre-excited), but not for CH_4[21,23]. We also address mechanistic aspects of the reaction, such as site-selectivity of the reaction, possible trapping mechanisms and their potential influence on the reactivity, the dependence of the reaction on initial molecular orientation, and the reactivity of methane on Pt(110)-(2x1) relative to Pt(111).

The rest of the paper is organized as follows. In Sections II and III we describe the theoretical and experimental methods employed in the current work, respectively. The results and discussion are presented in Section IV, before the conclusions are given in the final Section.

II. Theoretical Methods

The theoretical methods have been described in detail previously[21,23] and so only the most relevant details are presented here. At each collision energy, 1000 AIMD trajectories were run using the Vienna *ab-initio* simulation package (VASP) version 5.3.5[46–49]. For the Pt(110)-(2x1) surface, a (1x3) supercell was used as depicted by the solid lines in Fig. 1A, and nine layers were used with the bottom two layers held fixed in their bulk position. The first Brillouin zone was sampled using a 3x3x1 Γ-centered K-point grid, and the plane wave cut-off energy was set to 400 eV. Projector Augmented Wave (PAW) pseudopotentials[50,51] were used to represent the core electrons. In addition, a Fermi smearing with a broadening parameter of 0.1 eV was used to facilitate convergence. As shown in Tables SIII and SIV in the Supplementary Material, these parameters give a value of the activation barrier to better than within chemical accuracy of the more converged set-ups, although they lead to a slight overestimation (≈ 2kJ/mol) of the activation barrier for the lowest energy transition states.

As in previous work on CHD_3 dissociation on platinum surfaces[14,23,29,52], we make use of the SRP32-vdW exchange correlation functional, defined as[21]

$$\text{SRP32-vdW} = (1 - 0.32)E_X^{PBE} + 0.32E_X^{RPBE} + E_C^{vdW} \quad (1)$$

where E_X^{PBE} and E_X^{RPBE} are the PBE[17,18] and RPBE[20] exchange functionals respectively, and E_C^{vdW} is the van der Waals correlation functional of Dion et al.[53,54].

The CHD_3 molecule was placed 6.5 Å above the Pt(110)-(2x1) surface in a cell with a 13 Å vacuum between periodic replicas of the slab. As discussed previously[21,23] and in

Section SIII of the Supplementary Material, it was necessary to add 1.8 kJ/mol of translational energy to the molecule to account for the unconverged vacuum spacing. The initial velocities of the molecules were sampled from the distributions determined experimentally at nozzle temperatures of 500 K and higher (see Table SVI); the large number of trapped trajectories that we observed at 95.4 kJ/mol would reduce the value of making a comparison between the calculations and experiments at lower incident energies. The vibrational populations were sampled from a Boltzmann distribution at the nozzle temperature used to make the molecular beam expansion. Additionally, zero point energy was imparted to each of the vibrational modes of the molecule as the trajectories were run within a quasi-classical framework.

The trajectories were propagated using the velocity-Verlet algorithm in VASP with a timestep of 0.4 fs for a maximum time of 1 ps. A trajectory was considered reactive if one of the bond lengths (the dissociating bond) exceeded 3 Å, and scattered if the height of the CHD_3 above the Pt(110)-(2x1) plane was larger than 6.5 Å with the center of mass (COM) velocity directed away from the surface. If neither of these outcomes was observed during the maximum 1 ps propagation time, the molecule was considered to be trapped on the surface.

The reaction probabilities, p_{i}, were calculated from the AIMD calculations as

$$p_{\mathrm{i}} = \frac{N_{\mathrm{react}}}{N_{\mathrm{tot}}} \tag{2}$$

where N_{react} is the number of trajectories that react and N_{tot} is the total number of trajectories that were run for a given collision energy. The reaction probability that includes the contribution from trapped trajectories, $p_{\mathrm{i}}^{\mathrm{T}}$, was calculated in the same way, but the number of trapped trajectories was included in N_{react} (i.e., it was assumed all the trapped trajectories would go on to react). The statistical error bars, σ_{i} or $\sigma_{\mathrm{i}}^{\mathrm{T}}$, (which excludes or includes trapped trajectories) were calculated as

$$\sigma_{\mathrm{i}} = \sqrt{\frac{p_{\mathrm{i}}(1-p_{\mathrm{i}})}{N_{\mathrm{tot}}}} \tag{3}$$

and represent 68 % confidence limits.

III. Experimental Methods

The experiments reported here were performed in a molecular beam-surface science apparatus that has been described in detail previously[55]. Briefly, the machine consists of a three-fold differentially pumped molecular beam source coupled to an ultra-high vacuum (UHV) chamber with a base pressure of 5 x 10^{-11} mbar where the sample is located.

The continuous molecular beam was formed by skimming a jet expansion produced when a 1 % CH_4 in H_2 mixture of 1.6 bar stagnation pressure was expanded into the molecular beam source chamber through a 50 µm-diameter hole in a stainless steel nozzle. The translational energy of the molecular beam was controlled by resistively heating the nozzle between room temperature and 650 K, yielding translational energies between 58 and 125 kJ/mol. The velocity distribution of the molecular beam was measured by a time-of-flight method using a chopper wheel in combination with an on-axis quadrupole mass spectrometer (QMS).

The Pt(110)-(2x1) surface sample (Surface Preparation Labs, Zaandam) of 10 mm diameter was mounted between two tungsten wires attached to a liquid nitrogen cryostat. The surface temperature (T_S) could be controlled in the range between 90 and 1200 K using nitrogen cooling and by passing a DC current through the tungsten wires. In the experiments described in this work, depositions were performed at T_S = 650 K, which is above the desorption temperature of H_2[56] and CO[57,58], ensuring that the hydrogen carrier gas or any residual CO from the UHV background or molecular beam do not block sites on the Pt(110)-(2x1) surface. A Chromel-Alumel (K-type) thermocouple spot-welded to the surface was used to measure the sample temperature. Surface cleaning between measurements was done by performing Ar^+ sputtering and annealing cycles. The surface cleanliness was verified using

Auger Electron Spectroscopy, confirming that no detectable (< 1 % monolayer) trace of carbon or oxygen was on the surface.

The sticking coefficients were measured by the so-called King and Wells method[59] using an off-axis QMS to monitor the methane isotopologue parent mass at 19 amu. An example of a typical measurement trace is shown in Fig. 2A. The time axis has been shifted so that the molecular beam first impinges on the crystal at t = 0. Initially for t < -57 s, before the molecular beam enters into the UHV chamber, there is no detectable QMS signal for mass 19. At t = -57 s, a separation valve is opened and the molecular beam enters the UHV chamber leading to a rise in the partial pressure of 19 amu. For t < 0, an inert mica beam flag still blocks the molecular beam from reaching the reactive Pt(110)-(2x1) surface. At t = 0, the beam flag is raised, allowing the molecular beam to impinge on the clean reactive Pt surface. Any dissociation of CHD_3 on the Pt(110)-(2x1) surface results in a decrease of the 19 amu QMS signal. After 15 s deposition, the beam flag blocks the beam again, and at t = 64 s the separation valve is closed.

The time dependent sticking coefficient $S(t)$ was then calculated from:

$$S(t) = \frac{\Delta P(t)}{P} \tag{4}$$

where $\Delta P(t)$ is the change in the partial pressure of 19 amu for t > 0 when the flag is open and P the increase in 19 amu partial pressure when the molecular beam enters the UHV chamber and is scattered from the inert flag. $S(t)$ decreases with deposition time because the surface is being passivated by carbon atoms due to the dissociation of methane molecules. Figure 2B shows the corresponding $S(t)$ obtained from the QMS trace shown in Fig. 2A. The initial sticking coefficient S_0 for the clean surface was determined by fitting the $S(t)$ traces to a double exponential decay and using the fitting result for t = 0. A double exponential was used for the fits because the dissociative chemisorption of methane on a Pt(111) surface at a range of surface temperatures between 500 and 800 K had previously been shown to be

governed by two processes: a fast initial dissociation of the CH_4 and a slower growth of carbon particles on the surface[60]. Fitting $S(t)$ to a double exponential decay takes into account both processes.

IV. Results and Discussion

The experimental sticking coefficients (red) for CHD_3 dissociation on Pt(110)-(2x1) are compared with those obtained from the AIMD calculations using the SRP32-vdW functional (blue) in Fig. 3A. The calculated sticking coefficients are lower than the measured values. To quantify the disagreement between the experiments and calculations, the measured sticking coefficients were fit to an S-shape curve[61] (red line). The energy shifts of the calculated values away from the fit to the experimental data are given in kJ/mol in Fig. 3A, and the average value is 20.1 kJ/mol. This is almost a factor of 5 higher than the 4.2 kJ/mol which is commonly defined as chemical accuracy.

In Fig. 3B, we present a comparison of the measured (red) and calculated (green) sticking coefficients where the calculated S_0 were obtained assuming that all the trajectories which result in the CHD_3 being trapped on the surface after the 1 ps propagation time are reactive. The calculated values of S_0 should be considered as an upper limit since not all trapped trajectories must necessarily lead to dissociation. At the two lowest incident energies, if over half the trapped molecules do go on to react, the experimental and calculated reactivities would be in excellent agreement. However, previous work on Pt(211) suggests that it may well be the case that the majority of the trapped molecules will not react on Pt(110)-(2x1), with half of the molecules desorbing and no trapped molecules reacting when the trajectories were propagated for another 1 ps on Pt(211)[52]. In addition, even if all the trapped molecules were to react at the two highest incident energies, the calculations still underestimate the experimental sticking coefficients with an error that is larger than 4.2

kJ/mol. At these energies the uncertainty in the theoretical sticking coefficients is smaller, due to the lower number of trapped trajectories. Whilst it would be desirable to increase the range of the comparison, we did not go to higher incident energies as these would require experiments to be done at nozzle temperatures of greater than 650 K. These cannot be accurately modelled using quasi-classical AIMD trajectories because the population of excited C-D vibrational states becomes larger than 40 %, which can lead to artificial intramolecular vibrational energy redistribution (IVR) in the calculations[21] . In addition, comparing state-resolved experiments and calculations was not possible as the measurements would only be feasible at lower incident energies, where the larger trapping probabilities would lead to even greater uncertainty in the calculated sticking coefficients. In any case, the results that have been obtained suggest that the SRP32-vdW functional does not describe CHD_3 dissociation on Pt(110)-(2x1) within chemical accuracy. Additional reasons for the discrepancies found between the measured and computed sticking probabilities shown in Fig.3 are discussed further below.

A comparison of the sticking coefficients measured in the current study for the dissociation of CHD_3 on Pt(110)-(2x1) at T_S = 650 K with those from previous work for CH_4 dissociation at T_S = 600 K[42], T_S = 500 K[39] and T_S = 400 K[41,42] is presented in Fig. 4. The error bars on the data from reference 39 have been taken to be an absolute value of 0.02, which is the approximate value of the errors where they are reported. McMaster and Madix have shown that between surface temperatures of 500 K and 900 K, S_0 is independent of T_S for methane dissociation on Pt(110)-(2x1) at the high incident energies they considered ($\geq$ 75 kJ/mol)[39]. However, the comparison suggests that the sticking coefficients do decrease with surface temperature at E_i < 75 kJ/mol, with the two sticking probabilities measured at T_S = 400 K being smaller than values measured at 600 K. Whilst the error bars are large for the CH_4 data and the measurements were done at different T_S, S_0 tends to be smaller for CHD_3

than for CH_4, consistent with CD_4 sticking coefficients being smaller than those for CH_4 on Pt(111)[62]. Comparison of the new CHD_3 data with the previous data for CH_4 + Pt(110)–(2x1) for T_S = 500 K[39] and 600 K[42] suggests the new experiments to be accurate, and the problem in the comparison between the new experimental CHD_3 data and the theory (Fig.3) to lie in the calculations.

The uncertainty in the CH_4 sticking coefficients and the associated velocity distributions for the experimental data excludes the possibility of running AIMD calculations to determine if the SRP32-vdW functional reproduces the CH_4 reactivity data. In addition, the CH_4 experiments have mostly been done with higher nozzle temperatures which means that there will be a significant population of molecules in vibrationally excited states in the molecular beam expansion. In the AIMD calculations, these vibrationally excited molecules can undergo artificial IVR[21,23], which can result in (non-quantised) energy transfer between the bend and stretch vibrational modes causing the calculated sticking coefficient to be too high[21]. The CH_4 data is also only available in the energy range where the trapping probabilities are large in the AIMD calculations. Both of these factors would lead to a greater uncertainty in the calculated sticking coefficients which would reduce the value of any quantitative comparison between the published experimental data and AIMD calculations for CH_4.

As noted above we do not believe that including a trapping contribution to reaction would solve all the problems concerning the disagreement between theory and experiment. However, it is still useful to consider whether trapping mediated, or precursor mediated reaction might contribute to the sticking at low energies. For this, it is necessary to know the velocity of the trapped molecules parallel to the surface and their estimated residence time, so that we can estimate the distance travelled by the molecule during the trapping time on the surface. The velocity distributions of all the trapped molecules along the x-axis (perpendicular

to the rows of atoms in the surface, Panel A) and along the y-axis (parallel to the atomic rows, Panel B) were calculated from the AIMD results and are presented in Fig. 5. The distributions, $F(v)$ have been calculated using a Gaussian binning procedure as[52]

$$F(v) \propto \sum_{i}^{Nbins} \sum_{j}^{Ndata} \exp\left(-\frac{(b_0 + i\Delta b - v(j))^2}{2{\sigma_G}^2}\right) \quad (5)$$

where the sum runs over the number of bins (i) and number of data points (j), b_0 is the first value of v considered for the binning, Δb is the bin width (50 m/s) and σ_G is the standard deviation of the Gaussian used (100 m/s). Additionally, both of the distributions have been normalized such that the area is one. The figure shows that most of the momentum transfer occurs from normal to the Pt(110)-(2x1) surface to motion perpendicular to the atomic rows in the surface, i.e., from motion along the z-axis to motion along the x-axis in a so-called diffraction mediated pathway. This is due to the geometry of the surface, as has been observed previously in the trajectories which trap on Pt(211)[52]. The two peaks in the distribution in Panel A are due to the symmetry of the surface, and both are centered at significantly higher velocities than the velocity the molecule would have if it had fully equilibrated with the surface.

Whilst in this work we refer to the trajectories as trapped, it is important to make the distinction that they are still translationally hot, due to the propagation time limit of 1 ps. As shown in Panel B of the figure, the absolute values of the velocities of the molecules along the x-axis (i.e., perpendicular to the rows of atoms on the surface) are large, and larger than along the y-axis. Thus at least initially the trapped molecule should be viewed as a hot precursor exploring the surface in the direction perpendicular to the rows, and not as a physisorbed molecule accommodated on the surface. This means that one should be wary of applying theories assuming equilibrium (such as transition state theory) to calculating fractions of molecules that desorb or react; rather, this should be based on dynamics calculations.

The average time that the trapped molecules remain on the surface (τ_{trap}) at T_S = 650 K has been estimated using[63]

$$\tau_{\mathrm{trap}} = \left[\upsilon_{\mathrm{des}} \exp\left(\frac{E_{\mathrm{ads}}}{k_B T_S}\right)\right]^{-1} \quad (6)$$

where k_B is Boltzmann's constant, E_{ads} is the physisorption well depth which has been calculated to be 27.3 kJ/mol with the SRP32-vdW functional, and υ_{des} = 2.35 THz, the frequency of the frustrated translational mode perpendicular to the surface plane as obtained from a frequency analysis calculation for a relaxed methane molecule located at the physisorption minimum. Using Eq. (6), $\tau_{\mathrm{trap}} \approx$ 66 ps. During this time, it is possible that the trapped trajectories can sample a favorable (molecularly distorted or thermally distorted surface) geometry and react. Such trapping mediated dissociation has been measured previously at significantly lower incident energies ($\langle E_i \rangle$ < 10 kJ/mol) for methane dissociation on Pt(110)-(2x1) at surface temperatures of 400 K[40–42] and 600 K[42,43] where we estimate trapping times on the order of 1500 ps and 100 ps respectively using Eq. (6). Additionally, a trapping mediated dissociation channel has been reported for methane dissociation on Ir(111) at a surface temperature of 1000 K[64], where the average trapping time is 8 ps[65].

At low incident energies, a trapping mediated contribution to reaction may clearly be identifiable[40–43,64] for methane on Pt(110)-(2x1) through a decrease of the reaction probability with increasing incident energy. Walker and King observed this trend when measuring the reactivity of CH_4 on Pt(110)-(2x1) at low incident energies at different nozzle temperatures, with the sticking coefficient increasing with increasing nozzle temperature for the same value of incident energy[41]. Their explanation was that with increasing nozzle temperatures the molecules will have more vibrational excitation and that the additional vibrational energy leads to the increase in sticking coefficient, meaning that the vibrational lifetime of the vibrationally excited trapped molecules is shorter than, or of the order of the lifetime of the trapped molecules. In our case the vibrational lifetimes of the trapped molecules are expected

to be shorter (i.e., tens of ps[66]) than the estimated trapping time in our calculations (i.e., 66 ps). This implies that trapping mediated dissociation could be enhanced for initially vibrationally excited molecules, and that initial vibrational excitation could shift the balance between desorption and reaction of trapped molecules in the direction of more reaction.

At higher incident energies, trapping may continue to contribute to reaction even though the reaction probability rises with incident energy due to a dominant contribution of activated reaction. It is feasible that some of the trapped trajectories in our AIMD calculations for CHD_3 on Pt(110)-(2x1) could dissociate before desorbing, and that trapping contributes to reaction. We cannot confirm this as the 66 ps timescale is too long to run AIMD calculations for, due to the extra computational expense that would be required.

In the experiments, it is possible that trapped molecules encounter a higher order defect (e.g., a kink site) on the surface and dissociate, which is not modeled in the AIMD calculations. Assuming a small miscut of the Pt(110)-(2x1) resulting in a defect density of 1% and taking the average (absolute) velocity perpendicular to the steps of 24.3 Å/ps from the distribution in Fig. 5A, together with a trapping lifetime of 66 ps, the average trapped molecule will travel 1600 Å along the surface, which is almost 200 times the lattice spacing in x (≈ 1608 Å). Therefore on average, the trapped precursors encounter two higher order defects such as a kink site. Therefore, trapping mediated reaction at defects could in principle contribute to the sticking, and future calculations should address this possibility.

Additionally, it is possible in both experiments and calculations that the thermal surface atom motion leads to surface distortions that change the activation barrier for the reaction, with displacements of the surface atoms above the plane typically lowering the activation barrier[16,35,67,68]. For Pt(110)-(2x1), the lowering of the activation barrier is accompanied by the relaxation of many of the surface atoms, with the displacement of the ridge atom and the atom in the third layer below the ridge atom normal to the surface having

the greatest effect[33]. Whilst the change in barrier for individual atoms is comparable to that for flat surfaces, the cumulative effect for all the atoms in the Pt(110)-(2x1) surface has the potential to produce a large change in the activation barrier[33]. As the trapped molecules can sample several different distorted surface geometries with different activation barriers on subsequent impacts, this thermal motion provides a possible pathway for them to dissociate.

Both the dissociation sites and the initial impact sites for the trapped molecules are shown in Fig. 6 for all 4 000 AIMD trajectories that were run in the current study. Gray circles represent the surface atoms, with the ridge atom having the thickest outline (2nd column), then the facet and then the valley atom (4th column). The black circles present the initial co-ordinates of the trajectories that scatter, and the red, blue and green crossed circles the initial co-ordinates of the trajectories that react by C-H cleavage, react by C-D cleavage or trap. The red and blue solid circles represent the position of the COM of a reacting molecule when the C-H or C-D bond becomes longer than the transition state value (1.58 Å, see Table I) and the green solid circles the co-ordinate when the trapped molecule is closest to the surface on its first approach. The main dissociation site is the least co-ordinated ridge atom. This is shown to be the case at all the four collision energies that the trajectories were run at in Fig. 7A, which shows the fraction of dissociation that occurred on the ridge (red) and facet (blue) atoms at each incident energy. At all incident energies, a minimum of 90 % of the reactivity was on the ridge atom and no dissociation was seen on the valley atom. This agrees well with recent experiments performed for CH_4 on Pt(110)–(2x1), where dissociation is seen to occur only on the ridge atoms of the surface using site selective detection by Reflection Absorption Infrared Spectroscopy[69] and with previous work by Bisson et al.[42]. Figure 7B presents the same analysis as Fig. 7A, but for the trapped trajectories, which shows that as the incident energy increases the fraction of trapped molecules that first hit the ridge atom tends

to increase, although the analysis becomes less reliable at higher incident energies due to the lower number of trapped trajectories.

It is also evident from Fig. 6 that there is little or no steering during the course of the reactive trajectories, as the molecules that react dissociate at an xy-position that is similar to their xy-position at the start of the trajectory. The distances that all (red), the reacted (blue), and trapped (green) trajectories travel in the xy-plane (d_{xy}) during the propagation time are presented in Fig. 8. These have been calculated using an analogous expression to Eq. (5), but with $\Delta b = \sigma_G$ = 0.1 Å. The finite width of the Gaussian bin can lead to the values of the distribution being non-zero at unphysical (negative) values of d_{xy} but this is just an artifact of the binning procedure. Each of the three distributions presented in Fig. 8 has been normalized such that the area is one. The lack of steering for the reacted trajectories is also evident in Fig. 8, with the reacted molecules travelling an average distance of 0.49 Å in the xy-plane. Whilst this may seem to rule out a trapping mediated contribution to reaction, the maximum propagation time imposed on the AIMD trajectories (1 ps) means that the trapped molecules do not explore a large area of the surface; the average distance they cover is 20.56 Å after their first impact. In addition, the majority of the trapped trajectories impact the surface only once during the propagation time, as shown in Fig. 9. If the trajectories were propagated longer, they would impact the surface more than once and the distance they travel across the surface would increase; as stated above, trapped molecules could travel as far as 160 nm in 66 ps which is large enough for them to even encounter a defect in the experiment, which we did not model in the AIMD calculations. As the trapped molecules will travel large distances across the surface, they can sample many different sites, where they can then in principle dissociate, as discussed above.

The ridge atom, where most of the CHD_3 dissociation is found to take place (see Fig. 7A), is also the site on the surface where we find the lowest activation barrier (63.9 kJ/mol).

To locate the transition states, the dimer method was used as implemented in the VASP Transition State Tools package[70–73]. For these calculations, the Pt(110)-(2x1) surface was held in its relaxed, 0 K geometry. The initial molecular geometries were chosen to replicate the four transition states reported by Jackson and co-workers for the ridge atom[35]. We found that only two of these transition states (L2 and K1 using the nomenclature of references 35 and 33) were true first order saddle points in our calculations with the SRP32-vdW functional, and also that the L2 transition state is lower in energy than the K1 transition state. In addition, we found a third, higher energy transition state for dissociation on the facet atom, which we label TS3. The transition state geometries are shown schematically in Fig. 10 and the properties given in Table I. Whilst the energy of the four different transition states that Jackson and co-workers calculated using the PBE functional for methane dissociation on Pt(110)-(2x1) were the same within 2 kJ/mol, we find a bigger difference of almost 6 kJ/mol between the two transition states calculated with the SRP32-vdW functional. However, we find the geometry of the transition states calculated with the two functionals to be very similar. We also note that the transition state geometries on the Pt(111) and Pt(211) surfaces[52] more closely resemble the K1 geometry than the L2 geometry, which has the lowest barrier for methane dissociation on Pt(110)-(2x1) with the SRP32-vdW functional.

Having identified transition states, we now come back to explanations for the discrepancies between the measured and computed sticking probabilities presented in Fig.3. As discussed in Section SII of the SI, the TS energies are converged to within chemical accuracy with the input parameters used in the DFT calculations. However, convergence tests do suggest that if we were to converge the DFT calculations further by increasing the number of layers (to 22), the size of the unit cell (to 2x4), and the number of K-points (to 11x11x1), the L2 and K1 barriers would decrease by 2 and 3 kJ/mol, respectively. Modeling this effect

would increase the calculated sticking probabilities and lead to better agreement between the experiments and the calculations.

The SRP32-vdW functional may also overestimate the activation barrier height for CHD_3 dissociation on Pt(110)-(2x1) as functionals which include van der Waals correlation do not necessarily produce the correct geometry of the surface[74]. Table II presents a comparison of the difference between the bulk and surface geometry for the interlayer distances d_{ij} and the difference in height of the valley atom and the atom below the ridge in the third layer, b_3 calculated using the SRP32-vdW functional and from three experimental studies[75–77]. The distances are depicted in Fig. 1B. The SRP32-vdW functional seems to give a reasonable description of the distances d_{ij} but overestimates the value of b_3; even using the 22 layer slab gives a value of 0.32 Å. This suggests that in the calculations the facet atom is too high and the atom below the ridge atom is too low.

Previous work by Jackson and co-workers using the PBE functional has shown that the position of the atom below the ridge atom can significantly affect the activation barrier[33], with the electronic coupling, β_2, being 73.3 kJ/mol/Å for the K1 transition state, and 80.0 kJ/mol/Å for L2. If the SRP32-vdW functional overestimates b_3 by 0.2 Å (which is possible from Table II), then the atom below the ridge atom is 0.1 Å too low which very simplistically can lead to the calculated activation barrier for the L2 transition state being 8 kJ/mol too high and the K1 barrier being 7 kJ/mol too high, just considering the movement of the single atom. The final two columns of Table II show the activation barriers calculated for the L2 and K1 transition states using the SRP32-vdW functional and the relaxed experimental geometries. It should be noted that the lattice constant calculated using the SRP32-vdW functional (4.02 Å[23]) was used rather than the experimental lattice constant (3.92 Å[78]) to determine the geometries in the calculations, and for the medium energy ion scattering experiments, Δd_{34} = 1.1 % was assumed as a value is not given in reference 77. For two of the three experimental

geometries, the activation barriers for dissociation are lower than for the SRP32-vdW geometry, suggesting the calculated barriers could be too high which would lead to the sticking coefficients being too low. Further experimental studies into the geometry of the Pt(110)-(2x1) surface would be desirable to confirm if this might be the case.

The distributions of the angles that describe the geometry of the methane in the AIMD trajectories have been calculated using an equivalent expression to Eq. (5), but using a value of Δb of 1˚ and σ_G of 2˚. These are presented in Fig. 11 for θ (Panel A), β (Panel B) and γ (Panel C) for all trajectories at t = 0, (red dashed line), the reacted trajectories at t = 0 (blue dashed line) and the reacted trajectories at the time step where the dissociating bond becomes larger than the transition state value (t_{diss}, blue solid line). For the reacted trajectories, θ corresponds to the angle between the dissociating bond and surface normal, β the angle between the umbrella axis of the methyl and the surface normal, and γ the angle between the umbrella axis of the methyl and the dissociating bond (for a depiction of the angles, see Fig. 6 in reference 52). If the trajectories trap or scatter, the angles are defined in terms of the C-H bond and the CD_3 methyl group. The solid (dashed) black lines in the panels of the Figure correspond to the angles of the L2 (K1) transition state geometry. The initial distributions for θ and β both resemble sine distributions showing that the initial conditions are correctly sampled. As for methane dissociation on Pt(111)[52,79] and Pt(211)[52], Fig. 11A shows that the dissociating bond has to be oriented towards the surface for dissociation to occur, with the maximum reactivity seen around the value of θ for the L2 transition state.

Comparing the distributions of the angles at t = 0 with those at $t = t_{diss}$, the distribution for θ shifts towards smaller angles whereas the distribution for β shifts towards larger angles. Figure 11 shows that a rotationally sudden approximation for motion in θ should be more appropriate than a rotationally adiabatic approximation, but that some steering in θ does occur during reaction, as previously noted for CHD_3 + Pt(111)[80]. This suggests that

the reaction paths presented by Han et al. for CH_4 dissociation on Pt(110)-(2x1)[33], which makes use of the rotationally adiabatic approximation, may overestimate the sticking coefficients. The shifts in θ and β are accompanied by a change of the internal geometry of the molecules that dissociate, as shown in Fig. 11C.

Figure 12 presents a comparison of the experimental (Panel A) and calculated (Panel B) sticking coefficients for CHD_3 dissociation on Pt(111)[23] (black), Pt(211)[23] (red) and Pt(110)-(2x1) (blue). The Pt(111) data are for a surface temperature of 500 K, whereas the Pt(110)-(2x1) and Pt(211) data are for a surface temperature of 650 K. Sticking coefficient measurements for CH_4 dissociation on Pt(111) have shown that the reactivity does not change significantly between surface temperatures of 500 K and 800 K[60], and therefore the difference in surface temperature is unlikely to affect the reactivity trends for CHD_3 dissociation seen in Fig. 12. In Panel B the sticking coefficients assuming that all the trapped trajectories (after 1 ps) react are also shown for Pt(211)[23] (red open circles) and Pt(110)-(2x1) (blue open circles). Assuming that all the trapped trajectories go on to react leads to an apparent increase in some of these sticking coefficients as the incident energy is decreased (dotted lines). This does not mean that the calculations predict the sticking coefficients increase at lower incident energies as not all the trapped trajectories will necessarily dissociate, as discussed above. For Pt(211), the trapping probabilities were only significant at lower incident energies than in the current study for Pt(110)-(2x1), but it was possible to compare the calculated and measured sticking coefficients over a wider range of incident energies where the trapping probability was smaller, and the agreement between theory and experiment was found to be excellent[23]. It was not possible to increase the incident energy range in the current study as increasing the incident energy experimentally would require using a nozzle temperature above 650 K, where the population of C-D vibrations becomes significant (> 40 %). This can lead to artificial

intramolecular vibrational energy redistribution between the C-D bonds which can cause the quasi-classical AIMD calculations to overestimate the sticking coefficient[21].

At lower incident energies ($\langle E_i \rangle$ < 100 kJ/mol) the measured sticking coefficients are highest for the Pt(211) surface and lowest for the Pt(111) surface. This reflects the minimum energy barriers for each surface calculated using Eq. (S3), E_b^e, which is lowest for CHD_3 dissociation on the step edge atoms of Pt(211), and highest on the Pt(111) surface (the values are given in the fourth column of Table III). The difference in E_b^e for Pt(111) and Pt(110)-(2x1) is 14.7 kJ/mol, in excellent agreement with the 13.7 ± 2 kJ/mol estimated from experiments by Bisson et al.[42], although as noted previously the calculated Pt(110)-(2x1) barrier is likely to be too high. In the same work, the authors found the vibrational efficacy for CH_4 prepared in the antisymmetric stretch overtone to be slightly higher for Pt(110)-(2x1) than for Pt(111) which would suggest that the activation barrier is later on Pt(110)-(2x1) than on Pt(111). This is also captured in the geometries of the two transition states L2 and K1 calculated with the SRP32-vdW functional, with the activation barrier on Pt(110)-(2x1) having both a longer dissociating bond and being closer to the surface compared to that for Pt(111) (see Table III).

The relative reactivity of the surfaces changes at higher incident energies ($\langle E_i \rangle$ > 100 kJ/mol), with the Pt(111) surface being more reactive than the Pt(110)-(2x1) surface. McMaster and Madix reported the Pt(111) surface to be more reactive than Pt(110)-(2x1) for CH_4 dissociation at lower incident energies than here[39], but as shown in Fig. 13 the data for Pt(111)[81] they compared to[39] (black) are systematically higher than sticking coefficients measured by Bisson et al.[82] (blue), Luntz et al.[62] (green) and Chadwick et al.[60] (red) for the same system, with the reactivities from the latter three studies being in reasonable agreement (noting again that the differences in T_S are not expected to significantly affect the measured S_0[60]). This implies that the sticking coefficients for Pt(111) used by McMaster and Madix in

their comparison of the reactivities of CH_4 on the two surfaces are too large and that this is the reason for their different conclusion.

Extrapolation of the results for the Pt(211) surface to high energies actually suggests that the Pt(111) surface should be the most reactive of all three surfaces at the highest incident energies. The larger reactivity of the Pt(111) surface relative to that of the Pt(110)-(2x1) surface at high incident energies is observed in both the experimental and calculated sticking coefficients showing the SRP32-vdW functional correctly captures this trend. Whilst the Pt(211) and Pt(110)-(2x1) surfaces have lower activation barriers for CHD_3 dissociation than Pt(111), the atomic density of the sites with the lowest activation barrier (given in the fifth column of Table III) are lower for the stepped surfaces than for Pt(111). Additionally, the transition states at alternative sites on the stepped surfaces, for example the terrace atom on Pt(211) and the facet atom on Pt(110)-(2x1), have a higher activation barrier (given in the final column of Table III) for CHD_3 dissociation than on Pt(111). Once the molecules have sufficient incident energy on Pt(111) to overcome the barrier, they can react at any top site on the surface. The same is not true for Pt(211) and Pt(110)-(2x1), where only a fraction of the top sites on the surface have the lowest barrier, with other top sites having a higher barrier than on Pt(111). In the experiments, this leads to the sticking coefficients increasing more quickly for Pt(111) than for Pt(211) and Pt(110)-(2x1) and the Pt(111) surface being the most reactive at the highest incident energies. The sticking coefficients for Pt(211) are also consistently higher than Pt(110)-(2x1) in the energy range measured here as the lowest activation barrier for CHD_3 dissociation on Pt(211) is lower than on Pt(110)-(2x1) and the step edge atom density on Pt(211) is higher than the ridge atom density on Pt(110)-(2x1).

V. Conclusions

We have calculated sticking coefficients by running AIMD trajectories using the SRP32-vdW functional for CHD_3 dissociation on Pt(110)-(2x1) at a surface temperature of 650 K, and compared them to experimental results obtained by King and Wells measurements. The calculations underestimate the experimental sticking coefficients with there being an average energy shift of 20.1 kJ/mol between the two sets of data. There is, however, an uncertainty in the calculated sticking coefficients, particularly at the two lowest incident energies, due to the large number of trajectories where the CHD_3 molecules remain trapped on the surface (after 1 ps). The average trapping time of the CHD_3 on the Pt(110)-(2x1) surface at a temperature of 650 K has been estimated to be 66 ps. A trapping mediated dissociation pathway has been reported for methane dissociation on Ir(111) at a surface temperature of 1000 K[64] where the average trapping time is only 8 ps[65], suggesting that it is possible that a fraction of the trapped trajectories can go on to react. However, it is currently not possible to confirm whether the trapped trajectories do go on to react because it is not feasible to propagate the AIMD trajectories for these longer timescales, due to the extra computational expense that would be required.

At the two highest collision energies considered here, where the calculated trapping probabilities are lower, calculated sticking coefficients underestimate the experimental S_0 even if the assumption is made that all trapped molecules go on to react. It is not possible to confirm whether the calculations would also underestimate the sticking at even higher collision energies as the nozzle temperatures required to do the experiments would lead to a significant number of C-D vibrationally excited molecules (> 40 %), which can then undergo artificial IVR in the classical trajectory calculations. Unlike our previous studies[21,23], we were unable to compare state-resolved reactivities with the CHD_3 molecules prepared with a quantum of C-H stretch vibration as the trapping probabilities in the AIMD calculations

would still be large at collision energies where a significant population of C-H stretch excited molecules could be prepared experimentally. Future dynamics calculations will have to establish to what extent trapping in an initially hot precursor state, in which the molecule travels along the surface perpendicular to the steps, may enhance sticking, thereby reducing the difference between the calculated and measured sticking coefficients.

While trapping may promote reaction to some extent, it is clear that the SRP32-vdW functional does not describe the dissociation of CHD_3 on Pt(110)-(2x1) within chemical accuracy. The most likely reason for this is that the SRP32-vdW functional fails to accurately reproduce the interlayer relaxation and the intra-layer relaxation of the surface. The atom below the ridge atom is likely to be too far into the bulk, which causes the activation barrier for the dissociation to be too high by 6-10 kJ/mol, as suggested by calculations of barrier heights for two out of three experimental surface geometries.

In the AIMD calculations, the main dissociation site has been found to be over the least co-ordinated ridge atom in the surface, where we calculate the transition state with the lowest activation barrier. In our 1 ps simulations the trajectories where the molecules react are direct, and are initially oriented with the bond that dissociates towards the surface. Also, there is little steering of the molecules in either the angular degrees of freedom or the xy-plane. Trajectories that trap are most likely to impact first on the facet atom, and due to the geometry of the surface they tend to travel perpendicular to the atomic rows of the surface. This allows them to sample multiple sites on the surface during the time they are trapped, in which case they may go on to dissociate.

Supplementary Material

See supplementary material for a discussion of the preparation of the Pt(110)-(2x1) slab, convergence tests, residual energy correction and velocity distributions used in the AIMD calculations.

Acknowledgements

We gratefully acknowledge financial support from the Swiss National Science Foundation (grant Nos. P300P2-171247 and 178775/1), the Ecole Polytechnique Fédérale de Lausanne and the European Research Council through an ERC2013 advanced grant (No. 338580) as well as computer time granted by NWO-EW through a Dutch Computing Challenge Project grant. The authors thank Davide Migliorini for useful discussions.

References

[1] C.A. Wolcott, A.J. Medford, F. Studt, and C.T. Campbell, J. Catal. **330**, 197 (2015).

[2] A. Lozano, X.J. Shen, R. Moiraghi, W. Dong, and H.F. Busnengo, Surf. Sci. **640**, 25 (2015).

[3] X.J. Shen, A. Lozano, W. Dong, H.F. Busnengo, and X.H. Yan, Phys. Rev. Lett. **112**, 046101 (2014).

[4] P.M. Hundt, B. Jiang, M.E. van Reijzen, H. Guo, and R.D. Beck, Science **344**, 504 (2014).

[5] P.M. Hundt, M.E. van Reijzen, R.D. Beck, H. Guo, and B. Jackson, J. Chem. Phys. **146**, 054701 (2017).

[6] S. Nave, A.K. Tiwari, and B. Jackson, J. Phys. Chem. A **118**, 9615 (2014).

[7] A. Farjamnia and B. Jackson, J. Chem. Phys. **142**, 234705 (2015).

[8] B. Jiang, R. Liu, J. Li, D. Xie, M. Yang, and H. Guo, Chem. Sci. **4**, 3249 (2013).

[9] T. Liu, B. Fu, and D.H. Zhang, J. Chem. Phys. **149**, 054702 (2018).

[10] H. Guo, A. Farjamnia, and B. Jackson, J. Phys. Chem. Lett. **7**, 4576 (2016).

[11] R. Peverati and D.G. Truhlar, Philos. Trans. R. Soc. A Math. Phys. Eng. Sci. **372**, 20120476 (2014).

[12] K. Golibrzuch, N. Bartels, D.J. Auerbach, and A.M. Wodtke, Annu. Rev. Phys. Chem. **66**, 399 (2015).

[13] F. Nattino, H. Ueta, H. Chadwick, M.E. van Reijzen, R.D. Beck, B. Jackson, M.C. van Hemert, and G.J. Kroes, J. Phys. Chem. Lett. **5**, 1294 (2014).

[14] H. Chadwick, D. Migliorini, and G.J. Kroes, J. Chem. Phys. **149**, 044701 (2018).

[15] C. Díaz, E. Pijper, R.A. Olsen, H.F. Busnengo, D.J. Auerbach, and G.J. Kroes, Science **326**, 832 (2009).

[16] V.L. Campbell, N. Chen, H. Guo, B. Jackson, and A.L. Utz, J. Phys. Chem. A **119**, 12434 (2015).

[17] J.P. Perdew, K. Burke, and M. Ernzerhof, Phys. Rev. Lett. **77**, 3865 (1996).

[18] J.P. Perdew, K. Burke, and M. Ernzerhof, Phys. Rev. Lett. **78**, 1396 (1997).

[19] J.P. Perdew, J.A. Chevary, S.H. Vosko, K.A. Jackson, M.R. Pederson, D.J. Singh, and C. Fiolhais, Phys. Rev. B **46**, 6671 (1992).

[20] B. Hammer, L.B. Hansen, and J.K. Nørskov, Phys. Rev. B **59**, 7413 (1999).

[21] F. Nattino, D. Migliorini, G.J. Kroes, E. Dombrowski, E.A. High, D.R. Killelea, and A.L. Utz, J. Phys. Chem. Lett. **7**, 2402 (2016).

[22] L. Sementa, M. Wijzenbroek, B.J. van Kolck, M.F. Somers, A. Al-Halabi, H.F. Busnengo, R.A. Olsen, G.J. Kroes, M. Rutkowski, C. Thewes, N.F. Kleimeier, and H. Zacharias, J. Chem. Phys. **138**, 044708 (2013).

[23] D. Migliorini, H. Chadwick, F. Nattino, A. Gutiérrez-González, E. Dombrowski, E.A. High, H. Guo, A.L. Utz, B. Jackson, R.D. Beck, and G.J. Kroes, J. Phys. Chem. Lett. **8**, 4177 (2017).

[24] E. Nour Ghassemi, M. Wijzenbroek, M.F. Somers, and G.J. Kroes, Chem. Phys. Lett. **683**, 329 (2017).

[25] F. Nattino, C. Díaz, B. Jackson, and G.J. Kroes, Phys. Rev. Lett. **108**, 236104 (2012).

[26] E. Nour Ghassemi, M. Somers, and G.J. Kroes, J. Phys. Chem. C **122**, 22939 (2018).

[27] M. Wijzenbroek and G.J. Kroes, J. Chem. Phys. **140**, 084702 (2014).

[28] X. Zhou, F. Nattino, Y. Zhang, J. Chen, G.J. Kroes, H. Guo, and B. Jiang, Phys. Chem. Chem. Phys. **19**, 30540 (2017).

[29] H. Chadwick, A. Gutiérrez-González, D. Migliorini, R.D. Beck, and G.J. Kroes, J. Phys. Chem. C **122**, 19652 (2018).

[30] H. Chadwick, H. Guo, A. Gutiérrez-González, J.P. Menzel, B. Jackson, and R.D. Beck, J. Chem. Phys. **148**, 014701 (2018).

[31] N. Gerrits, D. Migliorini, and G.J. Kroes, J. Chem. Phys. **149**, 224701 (2018).

[32] M.A. Krzyzowski, P. Zeppenfeld, C. Romainczyk, R. David, G. Comsa, K.E. Kuhnke, and K. Kern, Phys. Rev. B **50**, 18505 (1994).

[33] D. Han, S. Nave, and B. Jackson, J. Phys. Chem. A **117**, 8651 (2013).

[34] R. Ducros and J. Fusy, Surf. Sci. **207**, L943 (1988).

[35] S. Nave, A.K. Tiwari, and B. Jackson, J. Chem. Phys. **132**, 054705 (2010).

[36] M.A. Petersen, S.J. Jenkins, and D.A. King, J. Phys. Chem. B **108**, 5909 (2004).

[37] M.A. Petersen, S.J. Jenkins, and D.A. King, J. Phys. Chem. B **108**, 5920 (2004).

[38] A.T. Anghel, D.J. Wales, S.J. Jenkins, and D.A. King, Phys. Rev. B **71**, 113410 (2005).

[39] M.C. McMaster and R.J. Madix, J. Chem. Phys. **98**, 9963 (1993).

[40] A. V Walker and D.A. King, Phys. Rev. Lett. **82**, 5156 (1999).

[41] A. V Walker and D.A. King, J. Chem. Phys. **112**, 4739 (2000).

[42] R. Bisson, M. Sacchi, and R.D. Beck, J. Chem. Phys. **132**, 094702 (2010).

[43] R. Bisson, M. Sacchi, and R.D. Beck, Phys. Rev. B **82**, 121404 (2010).

[44] M. Sacchi, D.J. Wales, and S.J. Jenkins, J. Phys. Chem. C **115**, 21832 (2011).

[45] M. Sacchi, D.J. Wales, and S.J. Jenkins, Comput. Theor. Chem. **990**, 144 (2012).

[46] G. Kresse and J. Hafner, Phys. Rev. B **49**, 14251 (1994).

[47] G. Kresse and J. Furthmüller, Comp. Mater. Sci. **6**, 15 (1996).

[48] G. Kresse and J. Furthmüller, Phys. Rev. B **54**, 11169 (1996).

[49] G. Kresse and J. Hafner, Phys. Rev. B **47**, 558 (1993).

[50] G. Kresse and D. Joubert, Phys. Rev. B **59**, 1758 (1999).

[51] P.E. Blöchl, Phys. Rev. B **50**, 17953 (1994).

[52] D. Migliorini, H. Chadwick, and G.J. Kroes, J. Chem. Phys. **149**, 094701 (2018).

[53] M. Dion, H. Rydberg, E. Schröder, D.C. Langreth, and B.I. Lundqvist, Phys. Rev. Lett. **92**, 246401 (2004).

[54] G. Román-Pérez and J.M. Soler, Phys. Rev. Lett. **103**, 096102 (2009).

[55] L. Chen, H. Ueta, R. Bisson, and R.D. Beck, Rev. Sci. Instrum. **84**, 053902 (2013).

[56] J.R. Engstrom, W. Tsai, and W.H. Weinberg, J. Chem. Phys. **87**, 3104 (1987).

[57] P. Hofmann, S.R. Bare, and D.A. King, Surf. Sci. **117**, 245 (1982).

[58] B.E. Hayden, A.W. Robinson, and P.M. Tucker, Surf. Sci. **192**, 163 (1987).

[59] D.A. King and M.G. Wells, Surf. Sci. **29**, 454 (1972).

[60] H. Chadwick, A. Gutiérrez-González, and R.D. Beck, J. Chem. Phys. **145**, 174707 (2016).

[61] A.C. Luntz, J. Chem. Phys. **113**, 6901 (2000).

[62] A.C. Luntz and D.S. Bethune, J. Chem. Phys. **90**, 1274 (1989).

[63] J. Frenkel, Z. Phys. **26**, 117 (1924).

[64] E. Dombrowski, E. Peterson, D. Del Sesto, and A.L. Utz, Catal. Today **244**, 10 (2015).

[65] G.O. Sitz and C.B. Mullins, J. Phys. Chem. B **106**, 8349 (2002).

[66] D.R. Killelea and A.L. Utz, Phys. Chem. Chem. Phys. **15**, 20545 (2013).

[67] S. Nave and B. Jackson, Phys. Rev. Lett. **98**, 173003 (2007).

[68] S. Nave and B. Jackson, J. Chem. Phys. **127**, 224702 (2007).

[69] A. Gutiérrez-González, M.E. Torio, H.F. Busnengo, and R.D. Beck, 'Site selective detection of methane dissociation on stepped Pt surfaces' (to be submitted).

[70] P. Xiao, D. Sheppard, J. Rogal, and G. Henkelman, J. Chem. Phys. **140**, 174104 (2014).

[71] A. Heyden, A.T. Bell, and F.J. Keil, J. Chem. Phys. **123**, 224101 (2005).

[72] G. Henkelman and H. Jónsson, J. Chem. Phys. **111**, 7010 (1999).

[73] J. Kästner and P. Sherwood, J. Chem. Phys. **128**, 014106 (2008).

[74] J. Klimeš, D.R. Bowler, and A. Michaelides, Phys. Rev. B **83**, 195131 (2011).

[75] P. Fery, W. Moritz, and D. Wolf, Phys. Rev. B **38**, 7275 (1988).

[76] E.C. Sowa, M.A. Van Hove, and D.L. Adams, Surf. Sci. **199**, 174 (1988).

[77] P. Fenter and T. Gustafsson, Phys. Rev. B **38**, 10197 (1988).

[78] J.W. Arblaster, Platin. Met. Rev. **41**, 12 (2006).

[79] G. Fűchsel, P.S. Thomas, J. den Uyl, Y. Ozturk, F. Nattino, H.D. Meyer, and G.J. Kroes, Phys. Chem. Chem. Phys. **18**, 8174 (2016).

[80] F. Nattino, H. Ueta, H. Chadwick, M.E. van Reijzen, R.D. Beck, B. Jackson, M.C. van Hemert, and G.J. Kroes, J. Phys. Chem. Lett. **5**, 1294 (2014).

[81] G.R. Schoofs, C.R. Arumainayagam, M.C. McMaster, and R.J. Madix, Surf. Sci. **215**, 1 (1989).

[82] R. Bisson, M. Sacchi, T.T. Dang, B. Yoder, P. Maroni, and R.D. Beck, J. Phys. Chem. A **111**, 12679 (2007).

TABLE I The bond length (r), height of the carbon above the Pt(110)-(2x1) plane (Z_C), angle between the dissociating bond and surface normal (θ), angle between the umbrella axis and surface normal (β), angle between the dissociating bond and umbrella axis (γ) and activation barrier calculated using Eq. (S3) (E_b^e) for the transition states given in the first column which are positioned above the atom given in the second column. The values in brackets correspond to those calculated using the PBE functional in a previous study by Jackson and co-workers[33].

Transition State	Atom	r (Å)	Z_C (Å)	θ (˚)	β (˚)	γ (˚)	E_b^e (kJ/mol)
L2	Ridge	1.58 (1.59)	2.16 (2.16)	118 (121)	147	30	63.9 (68.5)
K1	Ridge	1.57 (1.55)	2.26 (2.23)	131 (131)	165	34	69.8 (67.3)
TS3	Facet	1.56	2.05	128	148	33	94.8

TABLE II Comparison between the bulk and relaxed Pt(110)-(2x1) geometries obtained using the SRP32-vdW functional and those from previous low energy electron diffraction (LEED[75,76]) and medium energy ion scattering (MEIS[77]) studies, and the L2 and K1 activation barriers calculated using Eq. (S3) using the SRP32-vdW functional and the relaxed geometries given. The distances are depicted in Fig. 1B.

	Δd_{12} (%)	Δd_{23} (%)	Δd_{34} (%)	b_3 (Å)	L2 E_b^e (kJ/mol)	K1 E_b^e (kJ/mol)
SRP32-vdW	-18.5	-0.2	1.1	0.35	63.9	69.8
LEED[75]	-17.4	1.1	0.4	0.17	57.5	63.6
LEED[76]	-18.4	-12.6	-8.7	0.32	65.2	74.9
MEIS[77]	-16 (3)	4 (3)	N/A	0.10	54.8	60.1

TABLE III The bond length (r), height of the carbon above the surface plane (Z_C), lowest activation barriers calculated using Eq. (S3) (E_b^e), the density of the surface atoms with that activation barrier calculated using the experimental[78] (3.92 Å) (SRP32-vdW[23] (4.02 Å)) lattice parameter, and the next lowest activation barrier (E'^e_b) for the surfaces in the first column.

Surface	r (Å)	Z_C (Å)	E_b^e (kJ/mol)	Density (x10^{18}atoms/m^2)	E'^e_b (kJ/mol)
Pt(211)[52]	1.55	2.27	53.9	5.2 (5.1)	96.4
Pt(110)-(2x1)	1.58	2.16	63.9	4.6 (4.4)	94.8
Pt(111)[52]	1.53	2.29	78.6	15.0 (14.3)	N/A

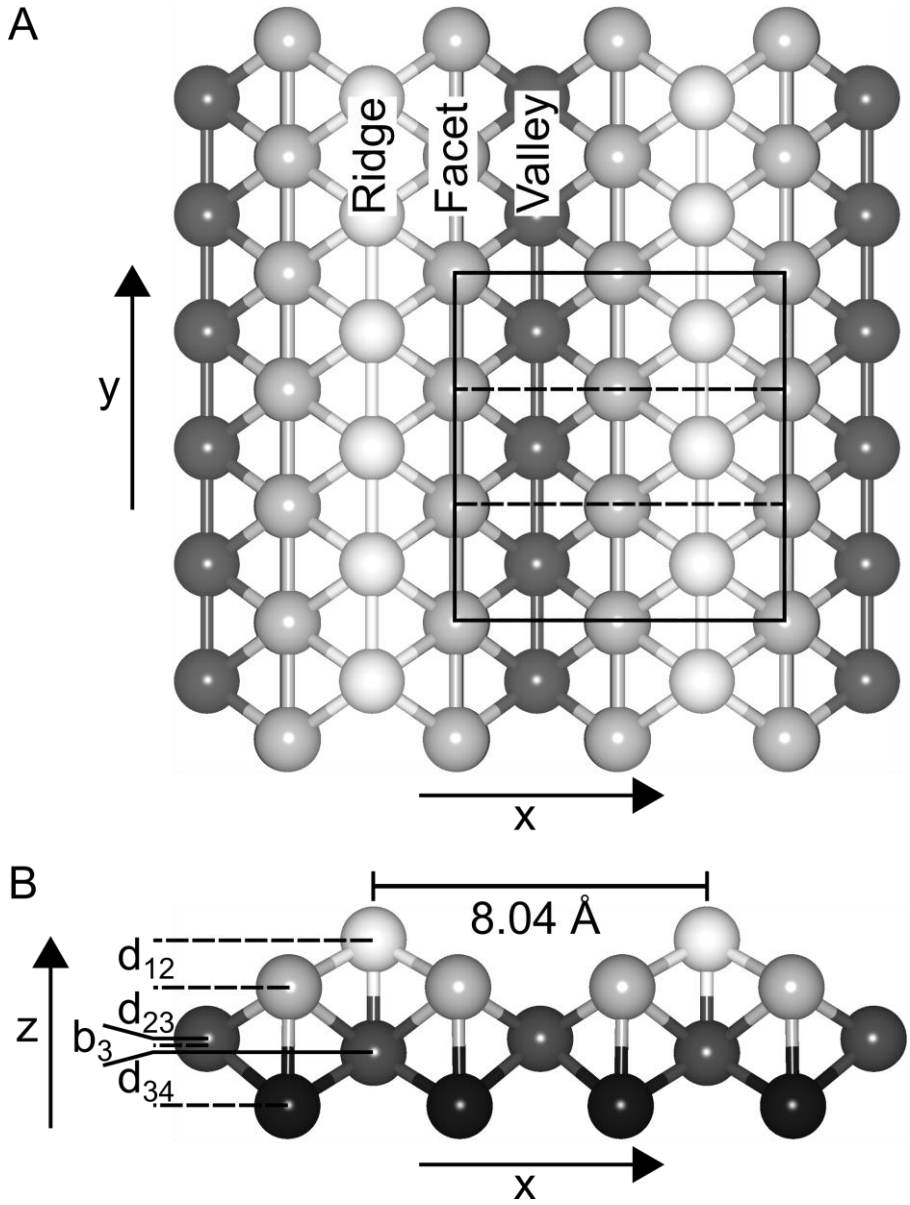

Figure 1 Panel A. Schematic top view of the Pt(110)-(2x1) surface showing the ridge, facet and valley atoms. The solid rectangle depicts the (1x3) supercell used in the AIMD calculations, and the dashed rectangle the unit cell. The x- and y-axes are shown as arrows. Panel B. Schematic side view of the Pt(110)-(2x1) surface showing the interlayer distances given in Table II. The x- and z-axes are shown as arrows. In both panels the atoms are in their relaxed 0 K positions.

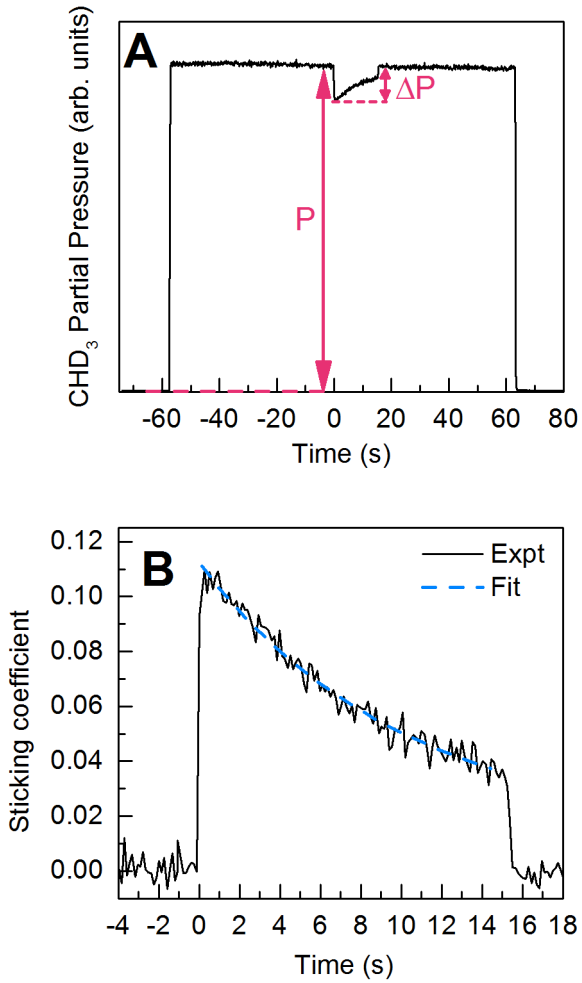

Figure 2 Panel A. King and Wells QMS trace for the dissociative chemisorption of CHD_3 on Pt(110)-(2x1) at an incident energy of 125 kJ/mol and a surface temperature of 650K. At time t = 0 the beam flag is moved and the molecular beam directly hits the Pt(110)-(2x1) surface. Panel B. Time dependence of the sticking coefficient calculated using Eq. (4). The dashed blue line corresponds to the fit to the data using a double exponential decay.

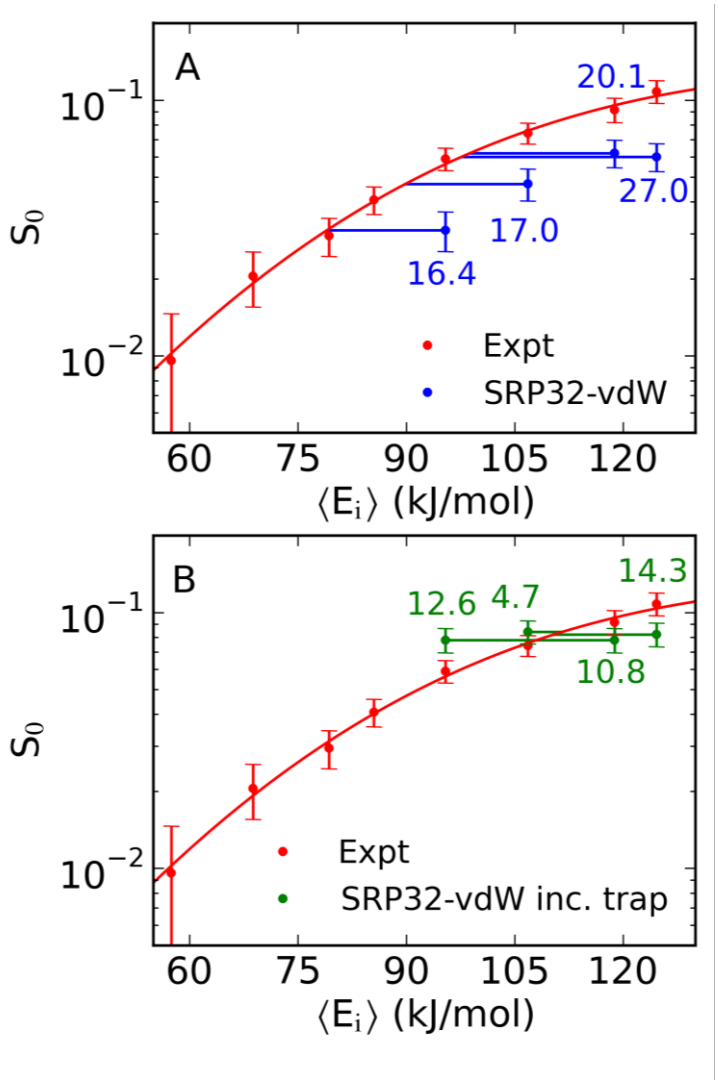

Figure 3 Panel A. Comparison of the experimental sticking coefficients (red) with those from the AIMD calculations excluding (blue) the trapped trajectories in the reaction probability for CHD_3 dissociation on Pt(110)-(2x1) at a surface temperature of 650 K. The red line shows an S-shape curve fit[61] to the experimental data, and the numbers the energy shift in kJ/mol between the calculated sticking coefficients and the fit. Panel B. As for Panel A, but the calculated sticking coefficients (green) include the contribution from all trapped trajectories.

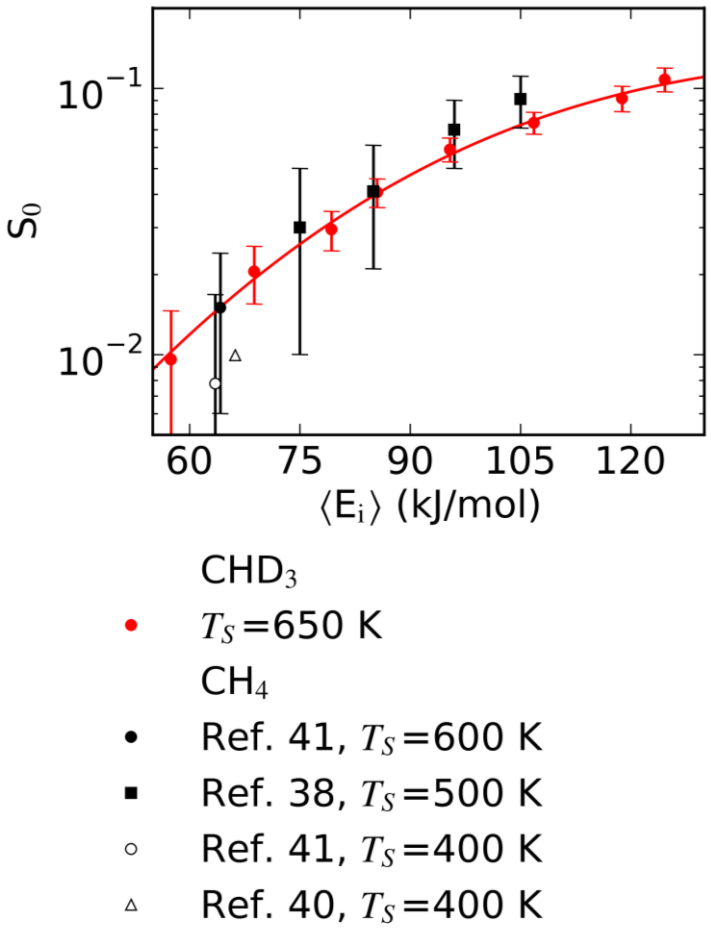

Figure 4 A comparison of the sticking coefficients for CHD_3 dissociation on Pt(110)-(2x1) measured in the current study at T_S = 650 K at nozzle temperatures (T_N) between 298 K and 650 K (red), with those measured previously for CH_4 dissociation at T_S = 600 K and T_N = 373 K[42] (black circle), T_S = 500 K and 610 K ≤ T_N ≤ 860 K[39] (black squares), T_S = 400 K and T_N = 373 K[42] (open circle) and T_S = 400 K and T_N = 800 K[41] (open triangle).

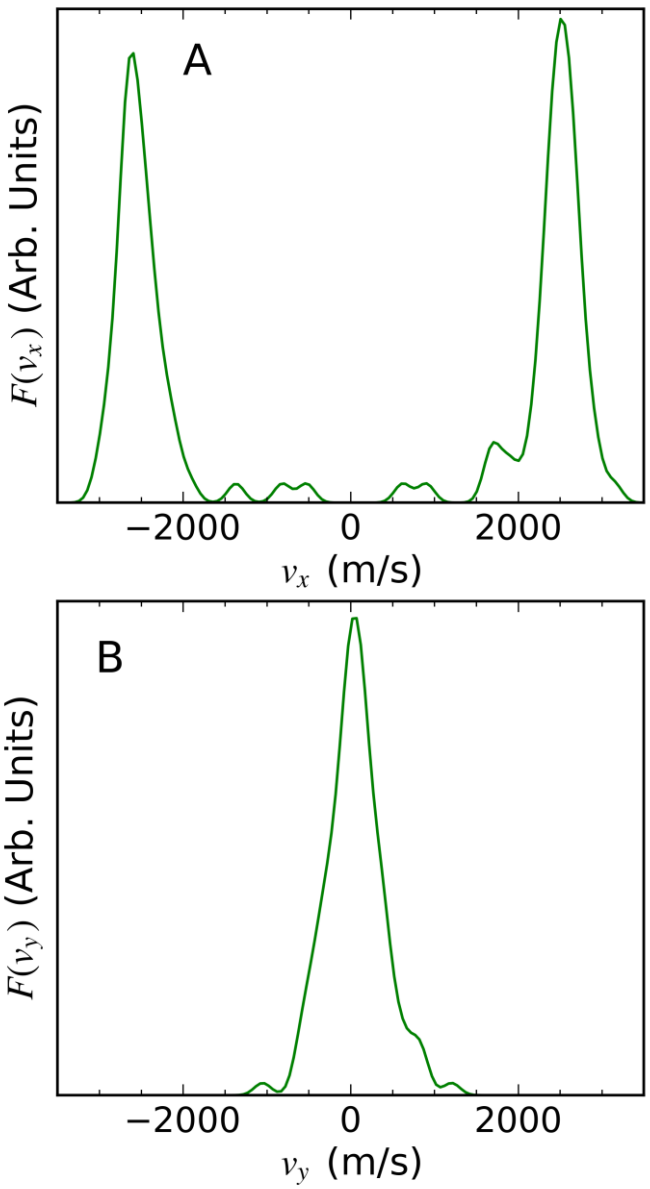

Figure 5 Panel A. Distributions calculated using Eq. (5) of the velocity of all the trapped molecules along the x-axis (perpendicular to the rows) after they have trapped. Panel B. As for Panel A, but along the y-axis (parallel to the rows).

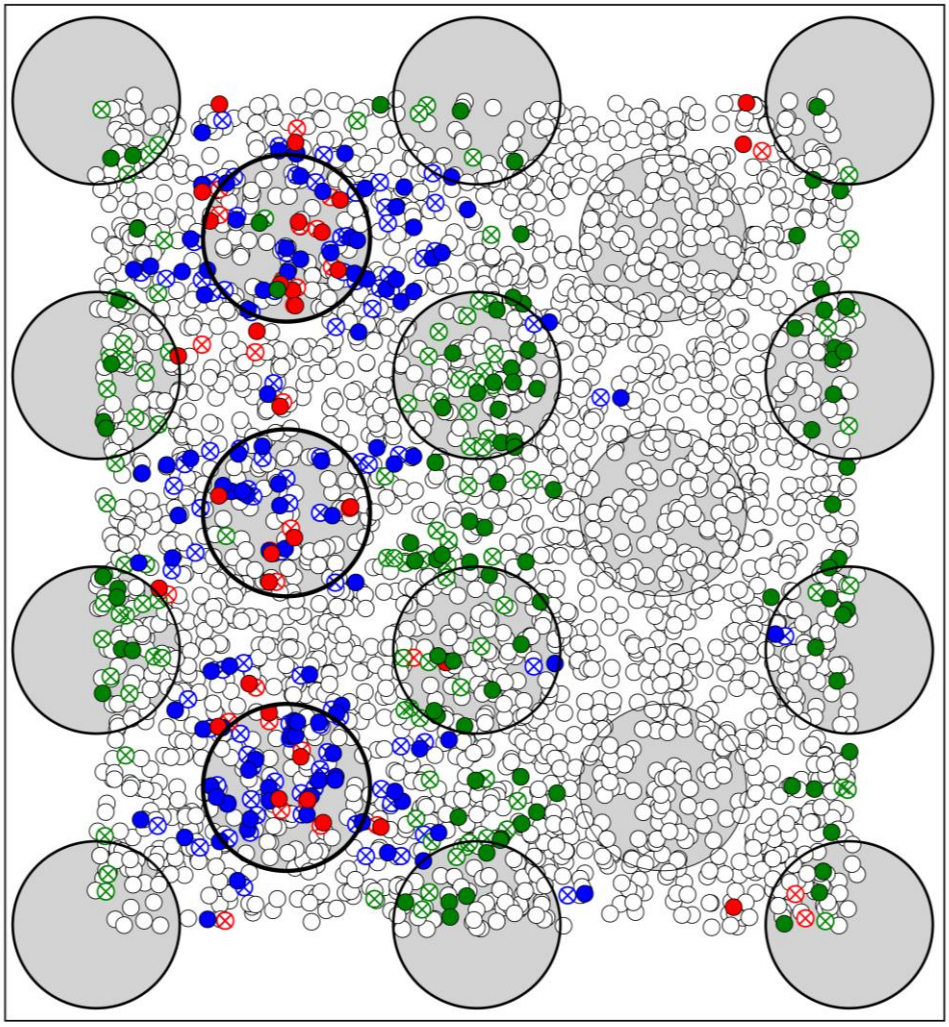

Figure 6 The initial positions of the center of mass (COM) of the molecule for all the scattered (open black), trapped (green crossed circles) and reacted (blue crossed circles for C-D cleavage and red crossed circles for C-H cleavage) trajectories. The solid symbols show the position of the COM when the C-H bond (red) or C-D bond (blue) becomes larger than the transition state value for the reacted trajectories, or at the point of closest approach on the initial impact for the trapped trajectories (green). The gray circles show the positions of the surface atoms, with those with the thickest outline (second column) being the ridge, and those with the thinnest outline (fourth column) the valley atoms. The other columns correspond to facet atoms.

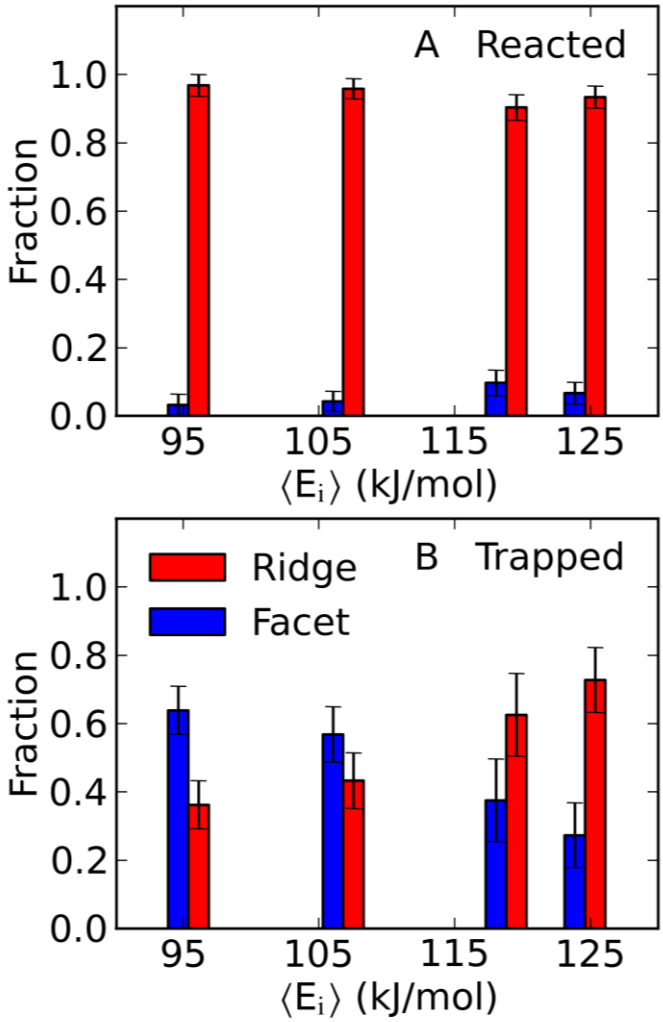

Figure 7 Panel A. Fraction of the reacted trajectories with the COM closest to the ridge (red) and facet (blue) atom when the dissociating bond becomes larger than the transition state value. Panel B. Fraction of the trapped trajectories with the COM closest to the ridge (red) and facet (blue) atom at the first impact on the surface.

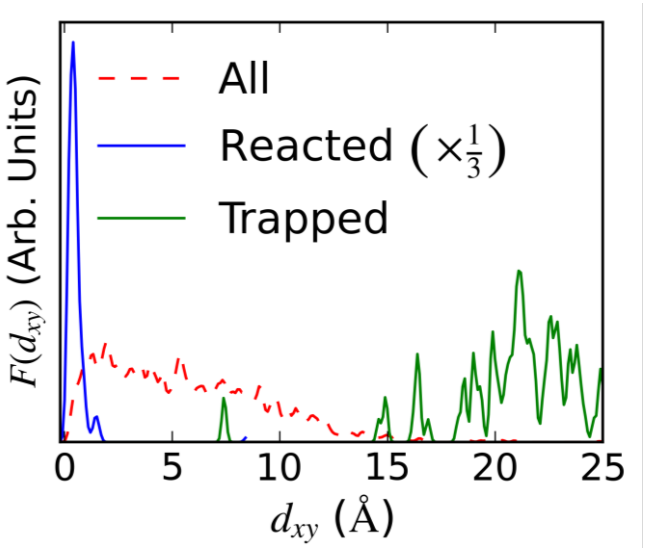

Figure 8 Distributions calculated using Eq. (5) for the distances in the xy-plane that all (red dashed), the reacted (blue) and the trapped (green) trajectories travel during the propagation.

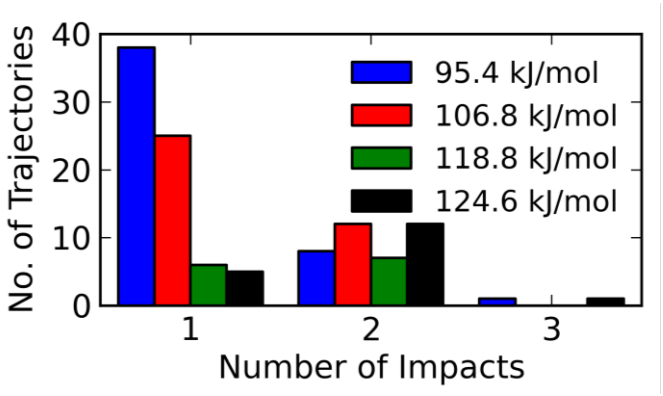

Figure 9 The number of times the CHD_3 molecules impact on the surface in the trapped trajectories during the 1 ps propagation time.

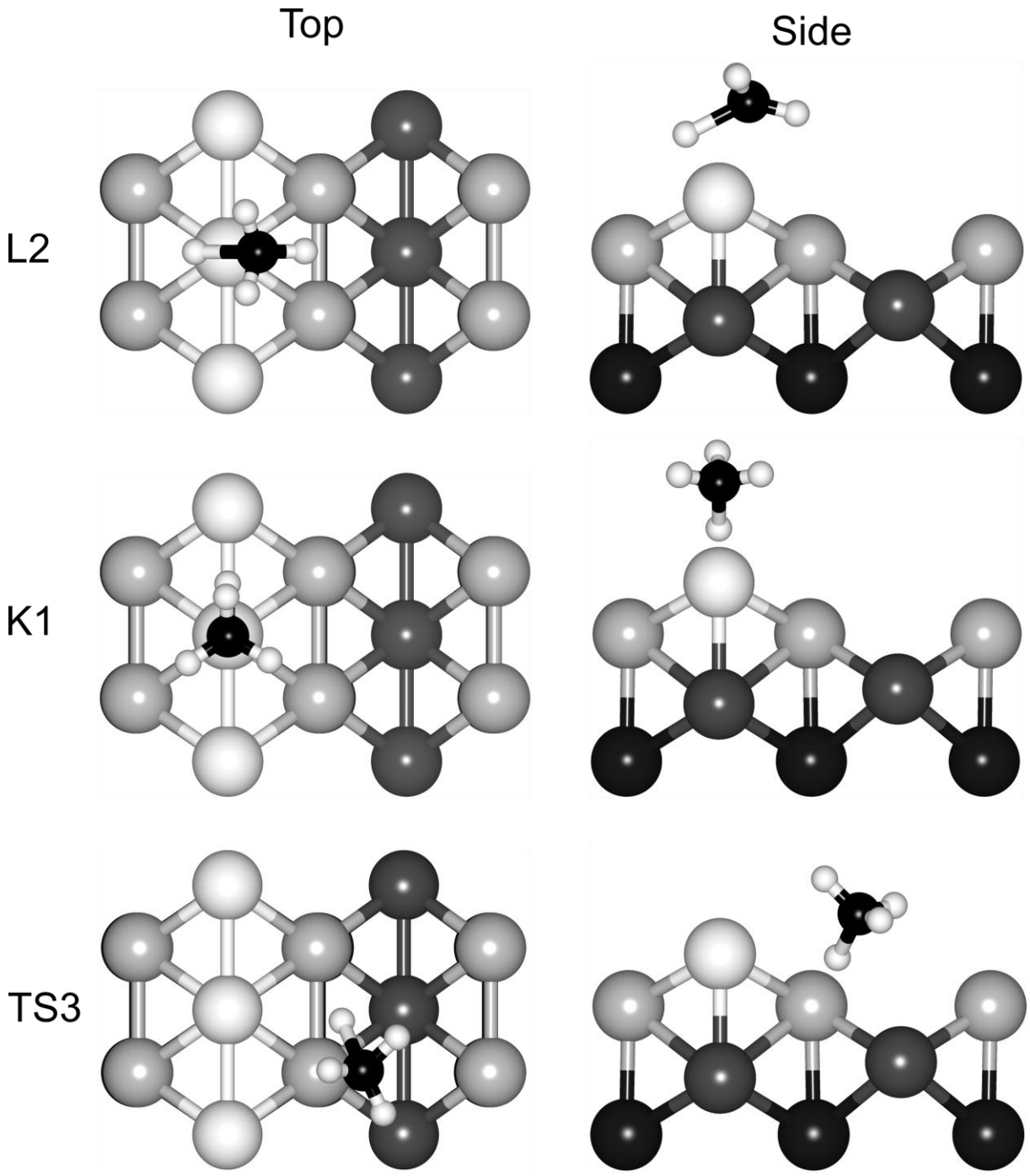

Figure 10 Top (left column) and side (right column) view of the L2 (top row), K1 (middle row) and TS3 (bottom row) transition states for methane dissociation on Pt(110)-(2x1).

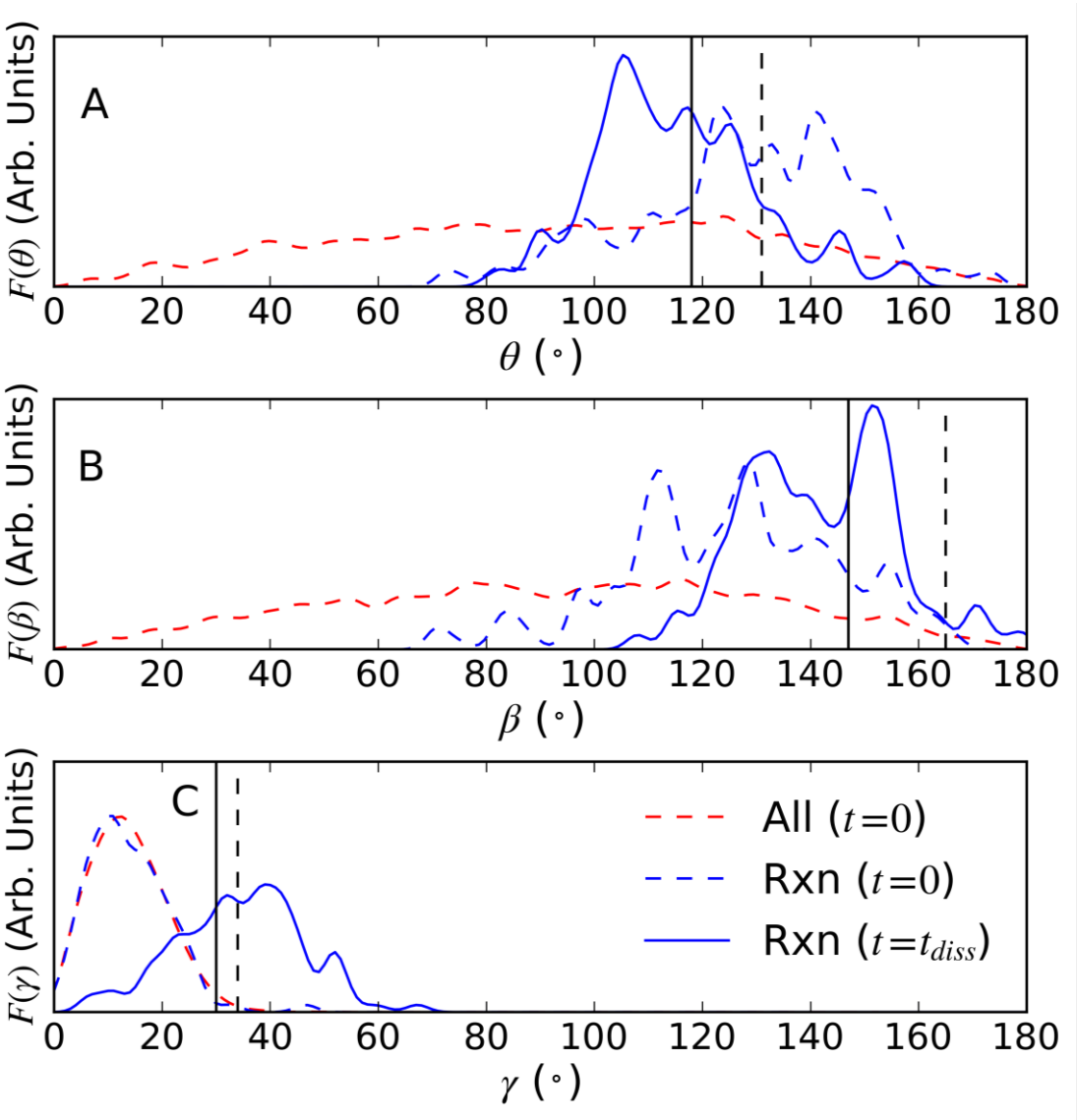

Figure 11 Panel A. The initial distribution of θ for all trajectories (red dashed line), initial distribution of θ for all the trajectories that react (blue dashed line) and the distribution of θ at the time when the dissociating bond becomes larger than the transition state value (t_{diss}, blue solid line). All distributions were calculated using Eq. (5). The solid black lines show the value of θ for the L2 transition state, and the dashed black lines θ for the K1 transition state. Panel B. As for Panel A, but for β. Panel C. As for Panel A, but for γ.

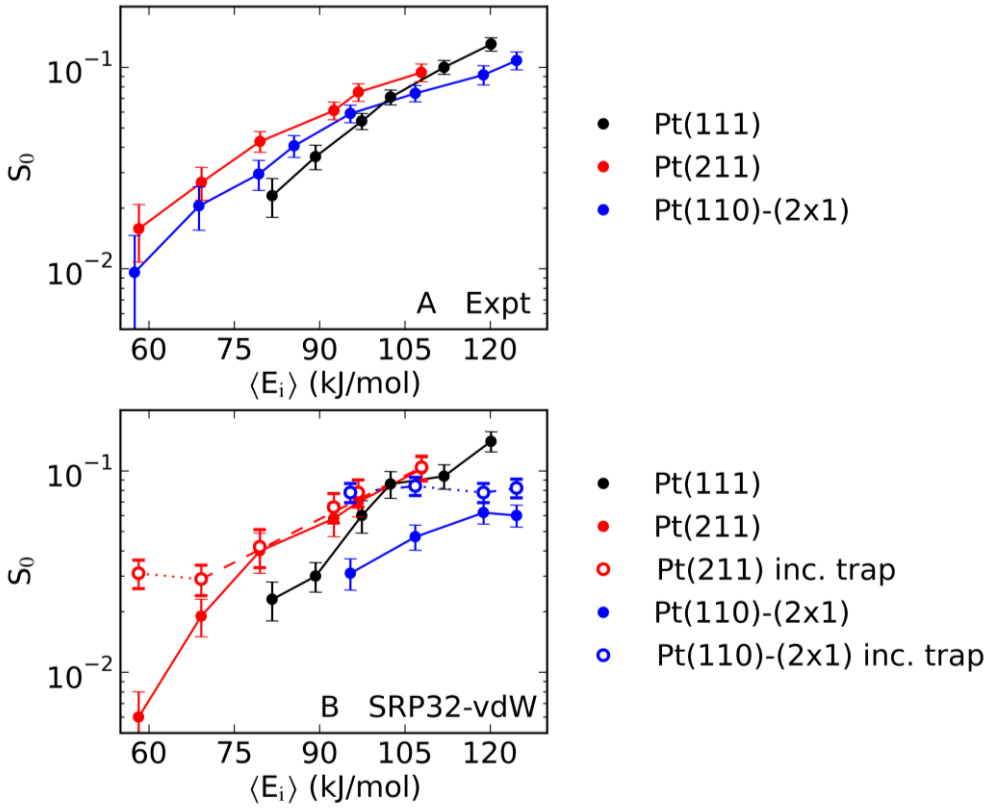

Figure 12 Panel A. Comparison of the sticking coefficients from King and Wells experiments for CHD_3 dissociation on Pt(111)[23] (T_S = 500 K, black), Pt(211)[23] (T_S = 650 K, red) and Pt(110)-(2x1) (T_S = 650 K, blue). Panel B. Comparison of the sticking coefficients from AIMD calculations using the SRP32-vdW functional for CHD_3 dissociation on Pt(111)[23] (T_S = 500 K, black), Pt(211)[23] including (red open circles) and excluding (red filled circles) trapped trajectories (T_S = 650 K) and Pt(110)-(2x1) including (blue open circles) and excluding (blue filled circles) trapped trajectories (T_S = 650 K). Lines have been added in both panels to guide the eye.

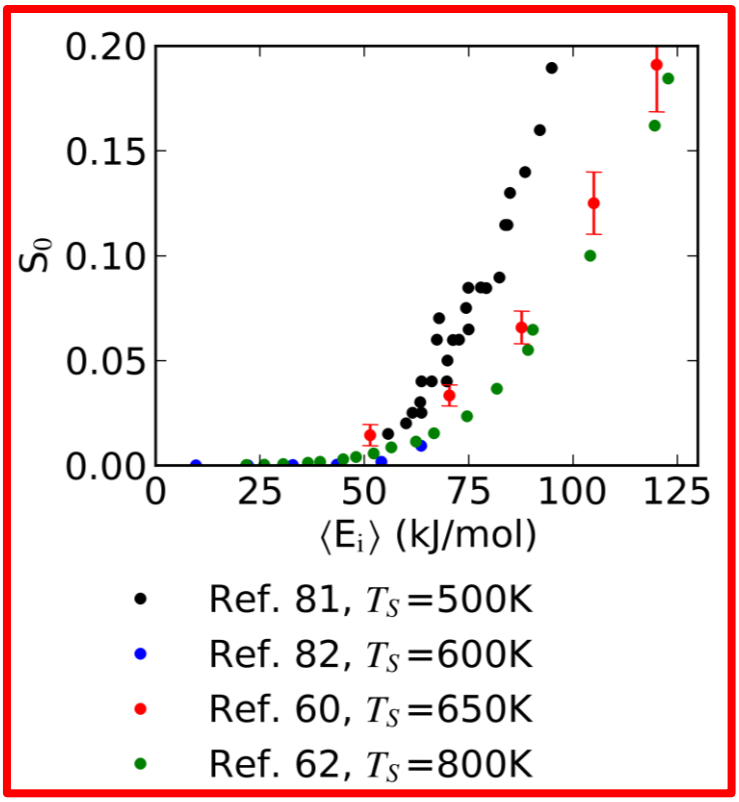

Figure 13 A comparison of the sticking coefficients for CH_4 dissociation on Pt(111) measured in previous studies by Schoofs et al. at T_S = 500 K[81] (black), Bisson et al. at T_S = 600 K[82] (blue), Chadwick et al. at T_S = 650 K[60] (red) and Luntz et al. at T_S = 800 K[62] (green).